Supplementary Information

Interlayer pillaring influences the octahedral tilting and electrochemical capacitance of tungsten oxides

Ran Ding, Michael A. Spencer, Noah P. Holzapfel, Matthew Chagnot, and Veronica Augustyn*

Department of Materials Science and Engineering

North Carolina State University, Raleigh, NC USA 27695

* Corresponding author: vaugust@ncsu.edu

Table of Contents

Table S1. Observed Raman peaks and assignments for $WO_3 \cdot 2H_2O$ and BA-WO_3.

Frequency (cm^{-1})	**WO_3**	**BA-WO_3**
2800-2900	--	*v*(C-H)
1470	--	*δ*(CH_2)
950	*v*(W-O_t)	*v*(W-O_t)
860, 890	--	*v*(W-O_t)
600-700	*v*(O-W-O)	--
330	*δ*(O-W-O)	*δ*(O-W-O)
210	lattice mode	lattice mode

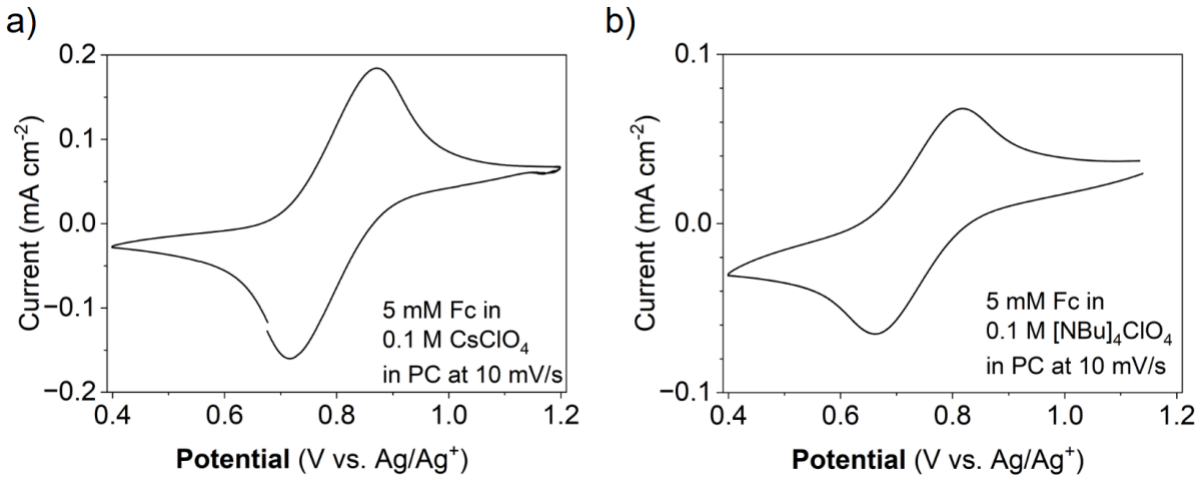

Figure S1. CV at 10 mV/s for 5 mM ferrocene (Fc) dissolved in (a) 0.1 M $CsClO_4$ in PC or (b) 0.1 M $[NBu]_4ClO_4$ in PC.

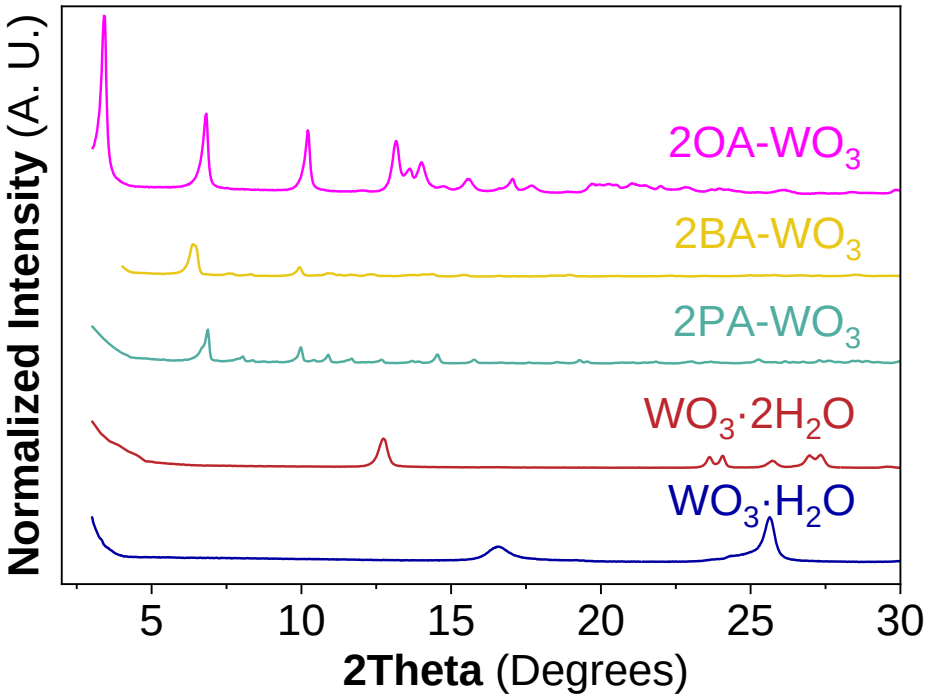

Figure S2. XRD of hydrated WO_3 and alkylammonium-cation pillared WO_3 with different alkyl chain lengths.

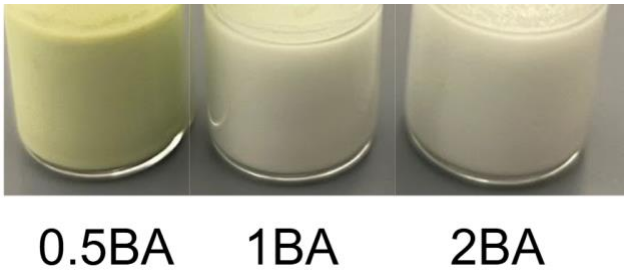

Figure S3. Different colors of BA-WO_3 due to different ratios of butylamine to $WO_3 \cdot 2H_2O$ during synthesis.

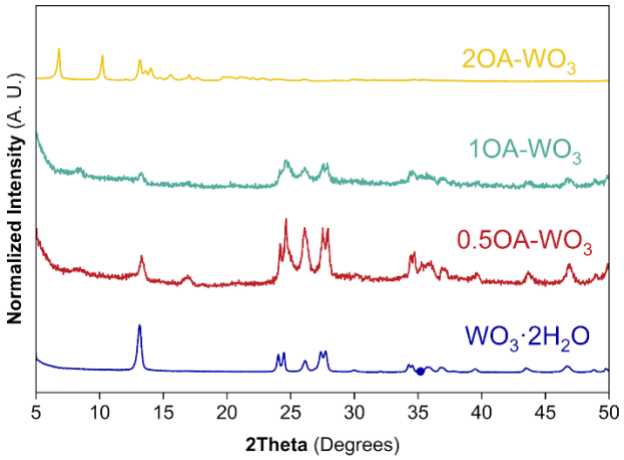

Figure S4. XRD of OA-WO_3 with various ratios between OA and WO_3.

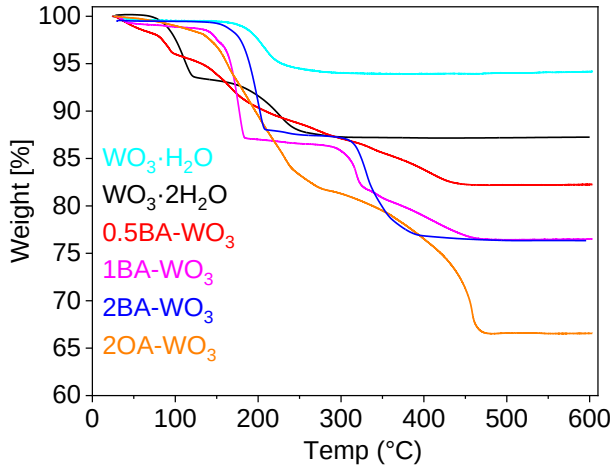

Figure S5. TGA curves for tungsten oxides hydrates ($WO_3 \cdot H_2O$, $WO_3 \cdot 2H_2O$), BA pillared tungsten oxides (0.5BA-WO_3, 1BA-WO_3, and 2BA-WO_3), and OA pillared tungsten oxides (2OA-WO_3). TGA measurements were performed in air with a heating rate of 2°C/min.

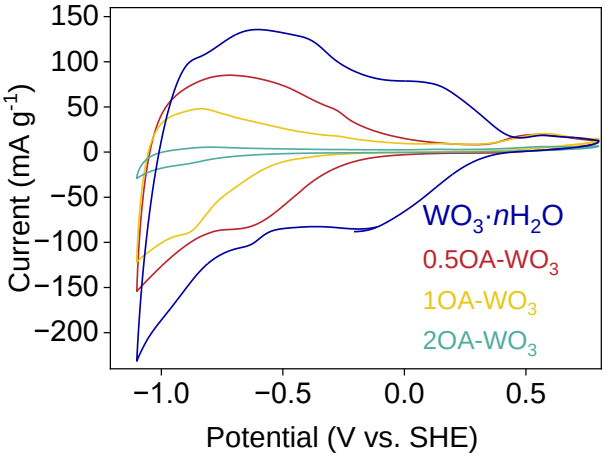

Figure S6. CVs at 1 mV/s of $WO_3 \cdot nH_2O$ and OA-WO_3 with various ratios between OA and WO_3 in 0.1 M $LiClO_4$ in PC.

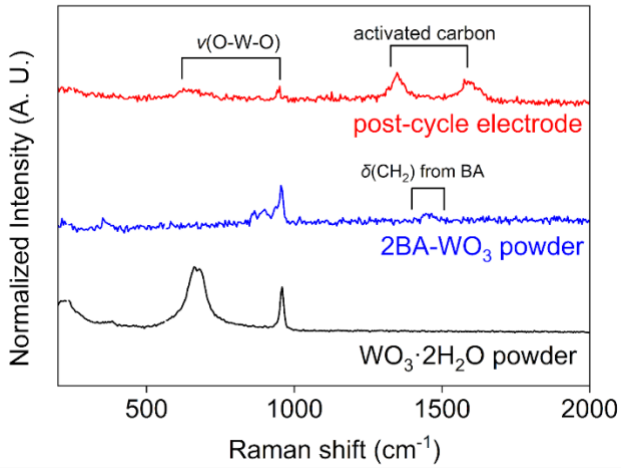

Figure S7. Ex situ Raman spectroscopy of an electrode consisting of fully BA-pillared tungsten oxide, 2BA-WO_3, after 250 cycles at 10 mV/s in 1 M H_2SO_4 and comparison to as-synthesized 2BA-WO_3 and $WO_3 \cdot 2H_2O$ powders.

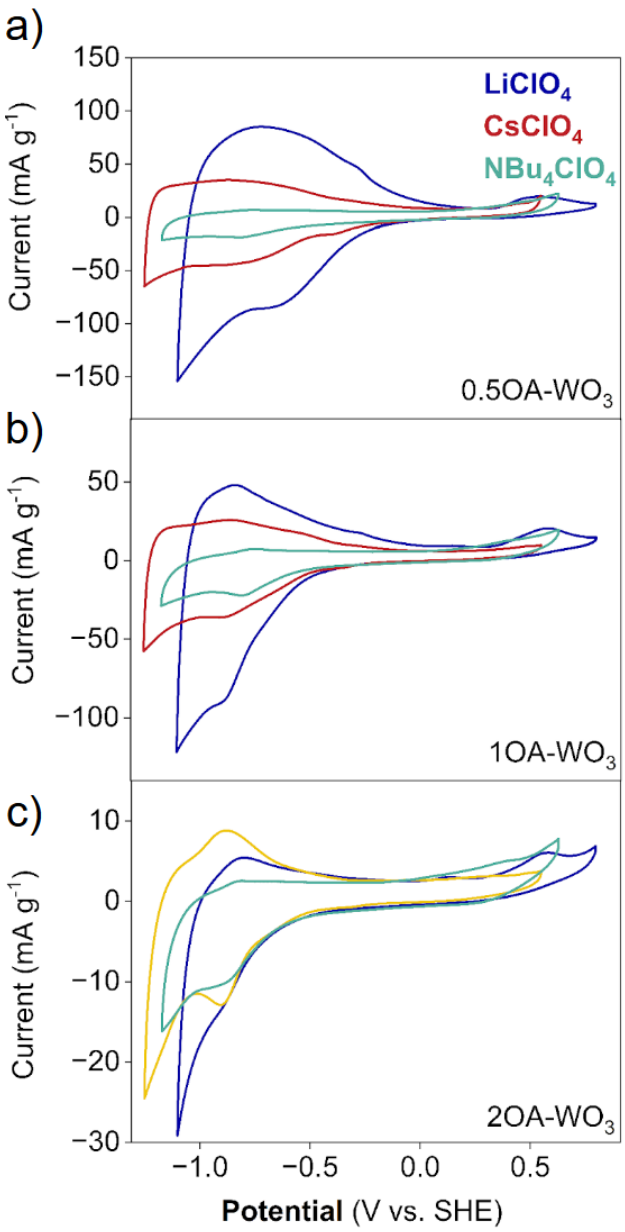

Figure S8. Comparison among CVs of OA-WO_3 with various ratios between OA and WO_3 in the solution of (a) 0.1 M $LiClO_4$, (b) 0.1 M $CsClO_4$ and (c) 0.1 M $[NBu]_4ClO_4$ in PC

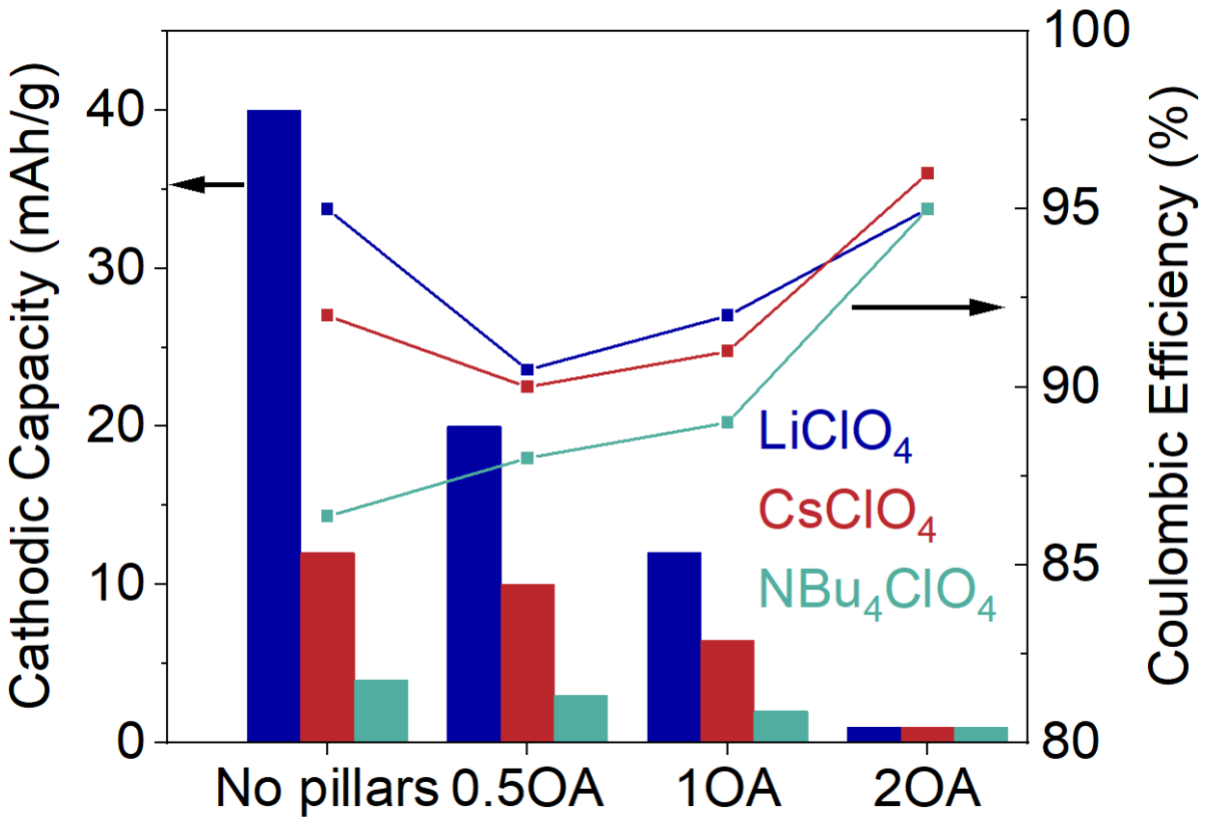

Figure S9. The capacity of $WO_3 \cdot nH_2O$ and 0.5OA-WO_3, 1OA-WO_3 and 2OA-WO_3 in different electrolytes. The bar graph is for cathodic capacity in left *y*-axis and scatter/line graph is for coulombic efficiency in right *y*-axis.

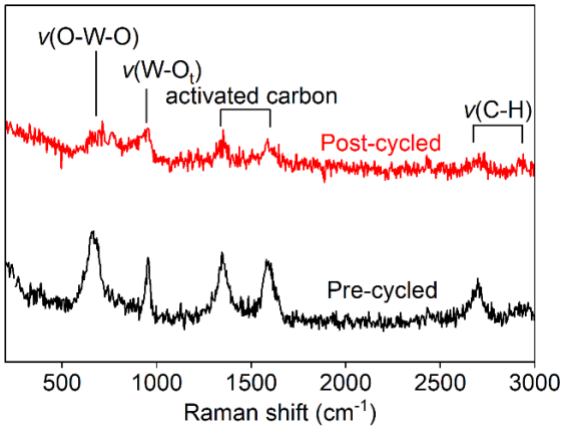

Figure S10. Ex situ Raman spectroscopy of a 0.5BA-WO_3 electrode before and after electrochemical reduction in 0.1 M $LiClO_4$ in PC to 2 V vs. Li/Li^+.

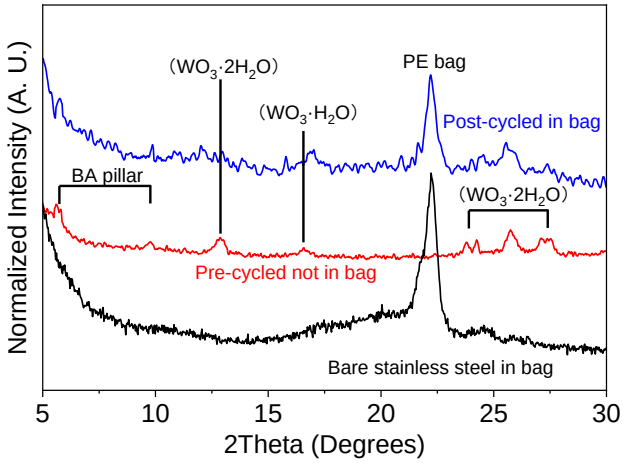

Figure S11. Ex situ XRD of 0.5BA-WO_3 before and after electrochemical reduction in 0.1 M $LiClO_4$ in PC to 2 V vs. Li/Li^+.

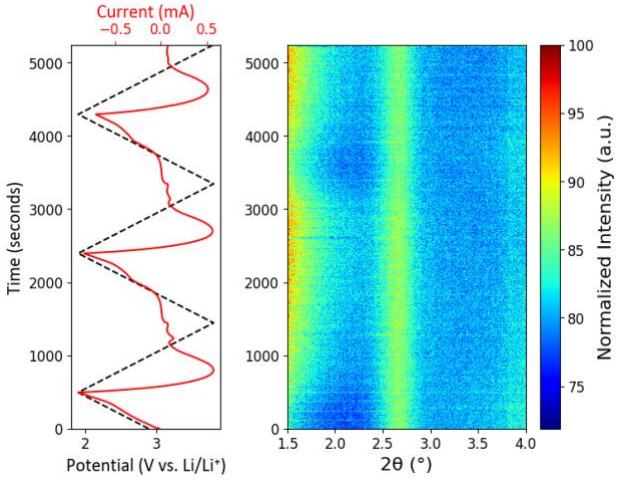

Figure S12. In situ electrochemical XRD of 0.5BA-WO_3 coated on stainless steel (SS) mesh in 0.1 M $LiClO_4$ in PC. Cyclic voltammetry was performed between 2 – 3.9 V at a scan rate of 2 mV/s.